Chapter 2

Materials and methods

This chapter covers materials selection, synthesis procedures, and characterization techniques that are used to design and characterize CB-like microstructure in ceramic systems. This thesis has chosen spinel-based and perovskite-based ceramic systems to shed some light on unexplored faces of the enigmatic self-assembled CB-like microstructure. Here the emphasis is to resolve obscurities that lingered for a long time. The foundation of this study has been laid with correlative microscopy based on TEM and APT. In such a correlative investigation, 2D information obtained by TEM complements corresponding 3D information gathered by APT. TEM analysis has been done in various modes, i.e. diffraction contrast, high-resolution phase-contrast, Z-contrast (HAADF-STEM-EDS), and convergent beam electron microscopy (CBED, i.e., Nano-Beam Diffraction). Since it was suspected that the evolution process is a series of phase transformations, XRD analysis has been utilized to track the phase evolution during the heat treatment process. To track the microstructural evolution, planned interrupted growth experiments have been performed at appropriate intervals. After each such interruption, samples were collected for further characterization, i.e., TEM, APT and physical properties characterization.

2.1 Materials selection

All the materials have been designed in such a way so that each of them may evolve with a particular type of CB-like microstructure that can help in resolving some of the ongoing issues in current technologies, i.e., magnetic memory recording trilemma [1], charge recombination and grain boundary hinderance in ASSLBs [2,3] (explained in chapter 1). In this thesis, attempts have been made to develop magnetic CB-like microstructure in Mn-doped $CoFe_2O_4$, $ZnGa_2O_4$, and $CoFeGaZnO_4$ for improved quality and quantity of magnetic data storage devices. Similarly, $LiLnTiO_3$-based perovskites have been developed with separate channels for improved ASSLBs.

2.2 Material synthesis

All the CB samples have been prepared by solid-state synthesis route due to its ease of material handling, cost-effectiveness, the certainty of the pure end product and success probability. Since CB-like microstructure evolves with a symmetry-breaking phase transformation, which turns a homogeneous compound into a well-organized mixer of two different phases, such microstructures can be obtained in some particular thermodynamic conditions. To achieve such thermodynamic conditions, composition and heat treatment has to be chosen in such a way so

that the system can be pushed to evolve as CB-like patterned microstructure with equal volume of two phases. This goal is achievable with a precise control over composition and heat treatment. Hence, the materials to be evolved as CB-microstructure were designed in particular stoichiometries.

2.2.1 Synthesis of CB-like microstructure in spinel manganites

Spinel manganite based CB structures have been synthesized with high purity precursors (>99.99 purity, Sigma Aldrich &Alfa Aesar), i.e., Co_3O_4 (II, III), Mn_2O_3 (III), Fe_2O_3 (III), Ga_2O_3 (III), and ZnO (II). Three different systems have been made (i) $Co_{0.6}Fe_{2-x}Mn_xO_{4+\delta}$ (ii) $Co_{0.6}Fe_{2-x}Mn_{x+y}GaZnO_{8+\delta}$ (iii) $ZnGa_{2-y}Mn_yO_4$, (where $\delta<<1$) in order to establish the correlation between crystal structure and evolution mechanism. To obtain CB-like microstructure in $Co_{0.6}Fe_{2-x}Mn_xO_{4+\delta}$, x = 1.6 was found to be the appropriate value of x. Similarly, for $Co_{0.6}Fe_{2-x}Mn_{x+y}GaZnO_{8+\delta}$, and $ZnGa_{2-y}Mn_yO_4$, x = 1.6 and y = 1 were found suitable for optimized CB-like microstructures. The intention of designing $Co_{0.6}Fe_{2-x}Mn_xO_{4+\delta}$ is to obtain two separate spinel phases with Fe-rich and Mn-rich compositions. Mixed powders were pelletized in a hydraulic hand press under a pressure of 5 Mpa. The Green pellets were sintered in the air in a covered Platinum crucible at 1250 ℃ for 24 hours, followed by quenching in ice water. This sintering process was repeated twice with an intermediate grinding of sintered and quenched pellets to ensure a homogeneous composition throughout the pellets. To obtain a diffusive rearrangement and expedite the diffusion kinetics, an ageing treatment was given in the air atmosphere at 375 ℃ for long hours. To closely investigate microstructural evolution, total time of heat treatment from quenching to equilibrium was divided into four slots, 0 hours, 5 minutes, 25 hours, 100 hours and 250 hours. The samples for XRD and TEM analysis were collected after each interruption.

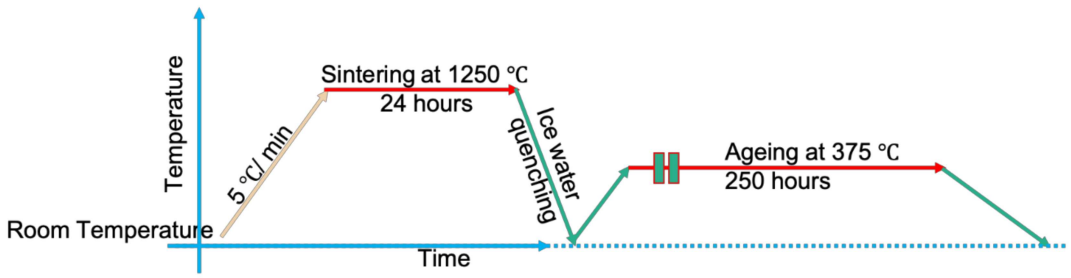

Figure 2.1: *Heat treatment program for all the manganite spinel systems.*

2.2.2 Synthesis of CB-like microstructure in $Li_{3x}Nd_{(2/3)-x}\square_{(1/3)-2x}TiO_3$

CB-like microstructure in perovskite systems consist of Li-rich and Li-lean domains and it is expected to facilitate channelized flow of the charge to avoid charge recombination and to resolve grain boundary hindrance. To obtained such microstructures in a $Li_{3x}Ln_{(2/3)-x}\square_{(1/3)-2x}TiO_3$ (Ln = La, Nd, Pr, and Sr) perovskite, $Li_{3x}Nd_{(2/3)-x}\square_{(1/3)-2x}TiO_3$ material is used. $Li_{3x}Ln_{(2/3)-x}\square_{(1/3)-2x}TiO_3$ is a A-site deficient compound where Li, Ln and vacancy are contesting for A-site. High purity precursors Li_2Co_3 (III), TiO_2 (IV) and Nd_2O_3 (III) were mixed in a precise $Li_{3x}Nd_{(2/3)-x}\square_{(1/3)-2x}TiO_3$ stoichiometry with x= 0.4, 0.8, 0.12, and 0.16. These values of x were chosen in such a way so that the composition can cover a range on phase diagram where maximum polymorphic phase transition can be studied. All the precursors were mixed properly in a mortar-pestle and were pressed in the form of a pellet by exerting 5 Mpa pressure with a hydraulic hand press. Subsequently, these pellets were solutionized at 1250 °C for 24 hours followed by annealing (20 °C/hours) till the temperature reached 500 °C (Figure 2.2). Afterward the samples were allowed to cool in air atmosphere. In addition, one pellet was directedly taken out from furnace in order to preserve a high symmetry C-phase (Pnma).

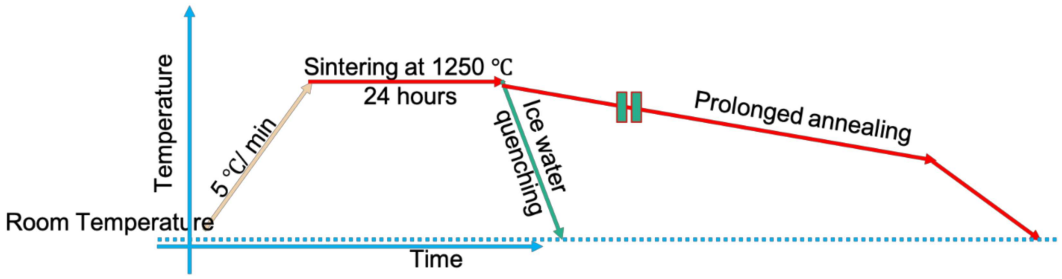

Figure 2.2: *Heat treatment to develop CB-like microstructure in* $Li_{3x}Nd_{(2/3)-x}\square_{(1/3)-2x}TiO_3$ *perovskite system.*

2.3 Characterization techniques

All the topological and morphological characterizations were designed in such a way so that the evolution of CB-like microstructure could be understood stepwise. Phase identifications and structural characterizations at the bulk level were performed with XRD analysis. To observe localized structural and compositional deviations, TEM investigations were performed. In addition, to construct a realistic 3D model of CB-like microstructure, TEM and

APT-based correlative microscopy was taken into account. To establish structure and property correlation, physical property characterizations before and after the evolution of CB-like microstructure were performed.

2.3.1 XRD analysis

X-ray diffraction analysis was performed with Cu-Kα radiation (λ= 0.154 nm) on a Rigaku Mini flex-600 operated at 40 kV-15 mA. The patterns were acquired using a slow scan rate (5º/minute) with a step size 0.02. Some XRD characterization were performed with Co-Kα (λ= 0.178 nm) on a Panalytical Empyrean High-Resolution X-ray Diffractometer operated at 40 kV- 40 mA. In this case, the scan rate was kept low at 2º/minute with a smaller step size of 0.01 degree to acquire more data points with higher sensitivity. This high-resolution data was used as input for multiphase Rietveld refinement performed on Fullprof software platform.

2.3.2 TEM analysis

TEM based comprehensive analysis provides a broader perspective of crystallographic, chemical, topological and morphological information about the sample. The correlation between this information may enable a better understanding of the intricate microstructures. Self-assembled CB-like microstructures have been reported to consist of two different types of basic building blocks made of similar shape, size and crystal structure. Diffraction contrast imaging (DCI) may visualize their topological arrangements from various crystallographic directions. The correlation between the diffraction patterns and corresponding bright/dark field images articulates the crystallographic relationship between various microstructural features. Their mutual orientation can be established through nano-beam diffraction patterns taken from individual features (basic building blocks). To do so, rotation calibration should be considered. For this study, rotation calibration was done with the help of ZnO nanowire (Figure 2.3). Since ZnO nanowire always grows along [0001] direction, an angular correlation has been made with various camera lengths at various magnifications. In addition to above-mentioned TEM techniques, this study also has utilized HAADF-STEM-EDS Z-contrast imaging that provides a compositional mapping of the microstructure. In addition, HR-phase contrast imaging at the interface to characterize the nature of the interface has been done. TEM characterizations have been done on Tecnai G^2 T20 and Titan 300 operated on 200 kV and 300 kV, respectively.

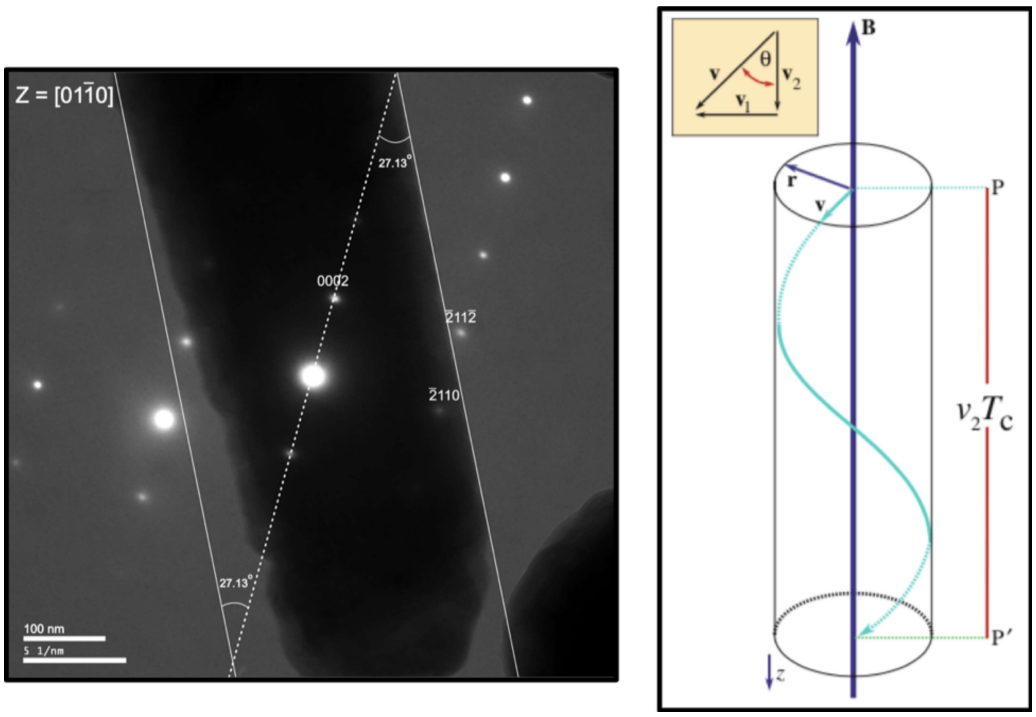

Figure 2.3: *Rotation calibration of Tecnai G² T20 TEM with the help of ZnO nanowire, Figure shows superimposition of diffraction pattern and the corresponding bright field image along* [01$\bar{1}$0] *zone axis. Schematic representation of e-beam travelling from filament to sample in a transmission microscope* [4].

2.3.3 APT analysis

APT facilitates a near atomic-scale 3D imaging with positioning and identity of individual atom (actually isotope). APT possesses the ability to tie chemical information to structure. It gathers realistic large-scale data that facilitates the extraction of a variety of information. 3D mapping provides latitude to create concentration profiles in any direction, volume, shape, size or normal to any defined surface. In these data sets, isoconcentration surfaces can be created to identify the concentration deviation of a particular atom/isotope. Interatomic positioning functions can be determined for studying ordering, dopant interactions, cluster formation, crystal structure, diffusion, and early stages of precipitation can be determined through intratomic inter-atomic distribution functions. This atomic distribution can be analyzed with super sensitivity, i.e., atom part per million (1 ppm).

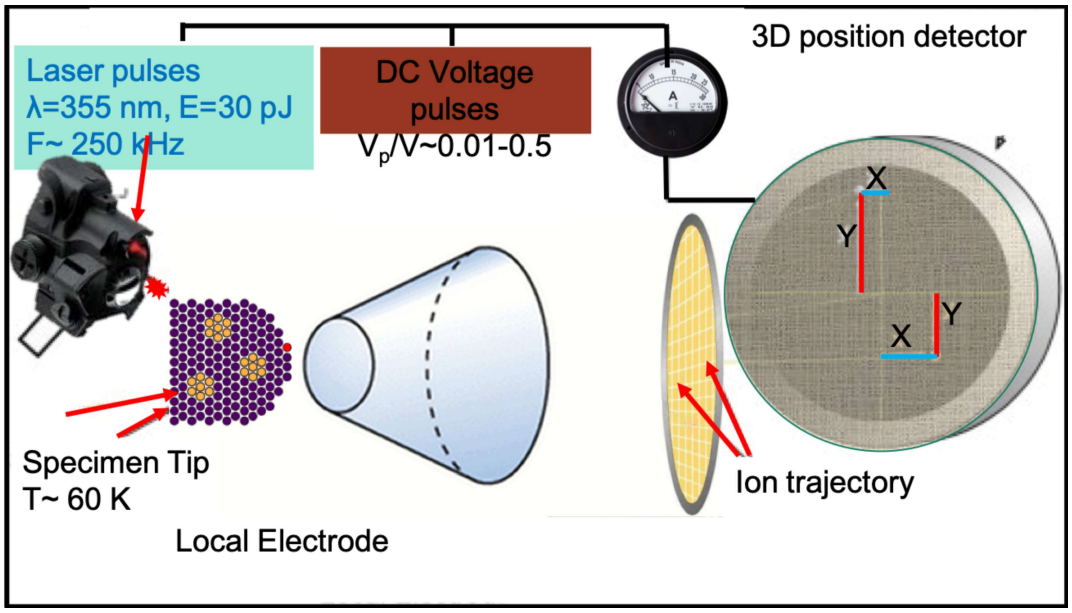

Figure 2.4: *Working line diagram of a Local Electrode Atom Probe.*

Atom probe tomography works on field evaporation due to the desorption and ionization of atoms under the influence of electrostatic force. An electron can be knocked out from outer orbital of the atom by a tunnelling process under an electric field greater than 10^{10} V/m. The electric field proportionally depends on the applied voltage and is inversely proportional to the tip curvature. Such a great tunnelling potential can be generated with a combination of 5-10 kV voltage and with a very sharp specimen (small tip radius). After stripping out the electron, atoms turn into positive ions and get accelerated towards the counter electrode. Thus, a specimen with a radius of curvature around 100 nm or less and a voltage around 10 kV accomplishes this task. APT, also termed as Local Electrode Atom Probe (LEAP), contains 3D detectors, laser optics, a sample stage, ion pump (Figure 2.4).

Once a surface atom gets knocked out in the form of ions, its identity can be determined by quantifying the time of flight (TOF). Parallelly, the position and TOF of each atom/isotope get recorded by position-sensitive detectors. As the tip gets consumed sequentially, a direct mapping of atoms at the curved apex is possible. The detector determines the x and y coordinates from the hit position on the detector and it determines the z coordinate from the evaporation sequence.

2.4 Sample Preparation

Samples collected at every interruption of the heat treatment were characterized with a planned correlative characterization strategy comprising of XRD, TEM and APT analysis. All the samples were prepared with standard techniques.

2.4.1 XRD sample preparation

XRD analysis of all the samples was performed on the pellets collected after every interruption of heat treatment. All the pellets were directly put into a Panalytical Empyrean high-resolution X-ray diffractometer operated at 40 kV voltage with 40 mA input current. For X-ray generation, a Co source with wavelength λ=0.178 nm was used.

2.4.2 TEM sample preparation

For TEM analysis, all the pellets were ground into fine powders, and were dissolved into pure ethanol to disperse the fine particles of maximum thinness before drop casting onto a carbon-coated copper grid. The solution was subjected to ultrasonication for about 20 minutes (Figure 2.3).

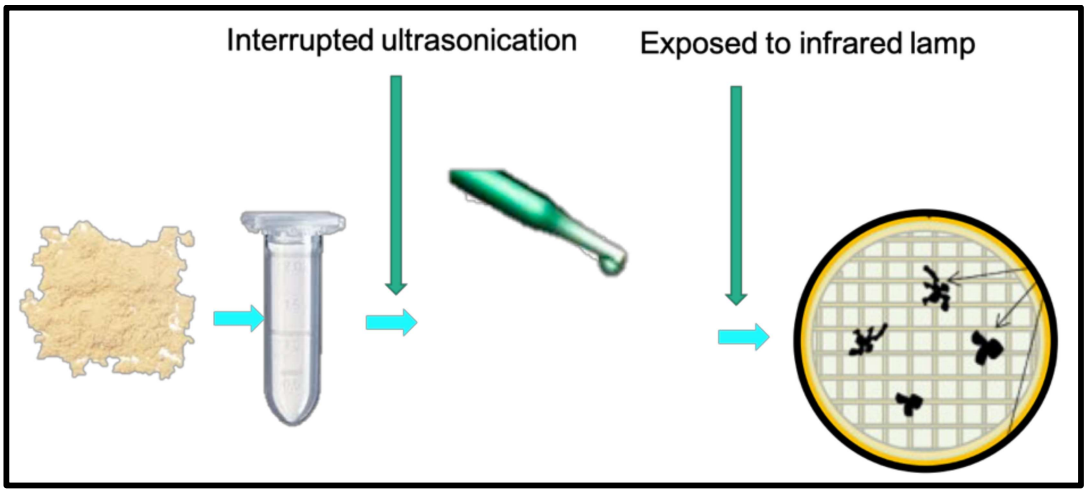

Figure 2.5: *TEM sample preparation by drop cast method.*

2.4.3 APT sample preparation

To prepare the tip for APT characterization, pre-characterized CB-samples were taken into account, and needle-shaped specimens were lifted out from vintage sites using a dual beam

workstation SEM–FIB (FEI Helios Nanolab G4UX). The process is explained stepwise in references (Figure 2.4) [5,6]. To minimize the Ga+ beam damage, a low-energy milling step (5 keV) was used at the final stage of sample preparation. APT measurements were performed in pulsing laser mode (wavelength of 355 nm (UV)) on Local Electrode Atom Probe (LEAP) 5000 XR, Cameca Instruments. During the whole process, the tip temperature was maintained at 60 K. The laser pulse frequency was set to 250 kHz with 30 pJ energy. The data collection rate was 0.5% ions per field evaporation pulse. The microstructural reconstruction and data analysis were performed on the Integrated Visualization and Analysis Software (IVAS 3.8.10) of Cameca Instruments Inc (Madison, WI, USA).

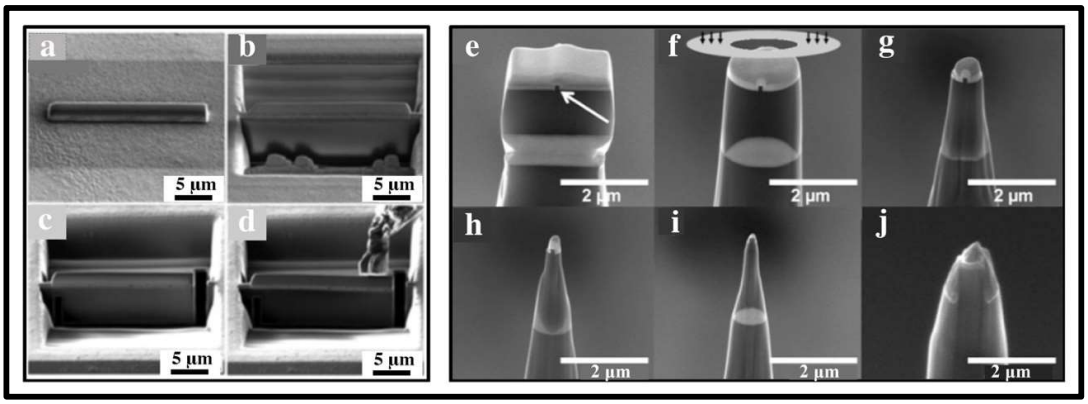

Figure 2.6: *Sample preparation steps for APT analysis (a-d) SEM image showing groove formation and lifting the area of interest (e-j) SEM image showing shaping of lifted sample by laser sharpening to obtain needle with a sharp apex.*

2.5 Physical properties characterization

This thesis is focused to elucidate the evolution mechanism of the CB-like microstructural evolution, hence most of the work is related to microstructural characterization. For $LiNdTiO_3$ the effect of CB evolution on electrochemical properties has been studied to bridge the gap between the microstructural characterization and physical properties characterization.

The electrochemical performance of the samples was evaluated against the Li reference electrode. To prepare the working electrodes based on the above materials, the corresponding powders were mixed with carbon black and PVDF with 8:1:1 weight ratio. Electrochemical cycling was performed within the voltage range of 0.01–3V (vs. Li/Li^+). The CVs were

measured between the potential range of 0.01-3V (Vs. Li/Li^+) at the scan rate of $0.1mVs^{-1}$ at 25°C. A detailed stepwise explanation is mentioned in chapter 5.

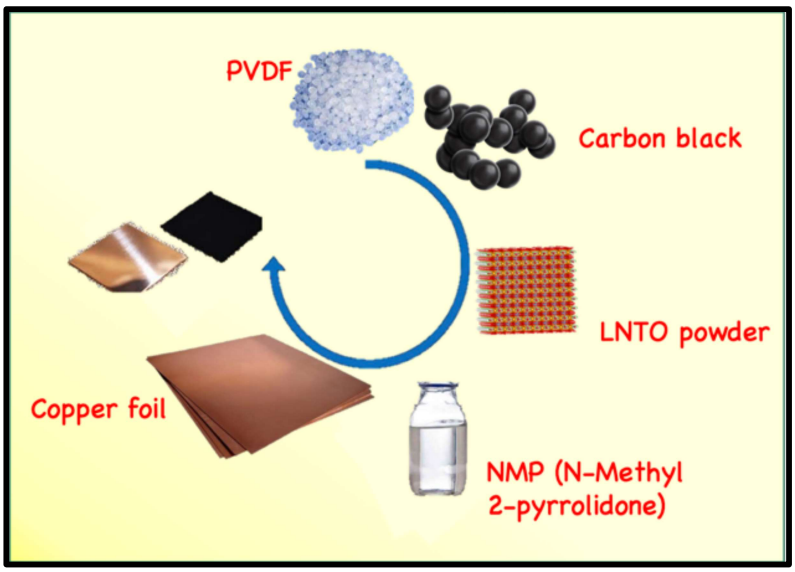

Figure 2.7: *Stepwise representation of sample preparation for electrochemical analysis of* $LiNdTiO_3$ *samples.*

References

[1] F.C. Gaspare Varvaro, Ultra-High-Density Magnetic Recording, Jenny stanford publishing, 2016. https://doi.org/10.1201/b20044.

[2] G.E. Blomgren, The development and future of lithium ion batteries, J. Electrochem. Soc. 164 (2017) A5019–A5025. https://doi.org/10.1149/2.0251701jes.

[3] C. Sun, J. Liu, Y. Gong, D.P. Wilkinson, J. Zhang, Recent advances in all-solid-state rechargeable lithium batteries, Nano Energy. 33 (2017) 363–386. https://doi.org/10.1016/j.nanoen.2017.01.028.

[4] C.B. Carter, D.B. Williams, Transmission electron microscopy, Springer International Publishing, Cham, 2016. https://doi.org/10.1007/978-3-319-26651-0.

[5] H. Zhang, K.G. Pradeep, S. Mandal, D. Ponge, H. Springer, D. Raabe, Dynamic strain-induced transformation: An atomic scale investigation, Scr. Mater. 109 (2015) 23–27. https://doi.org/10.1016/j.scriptamat.2015.07.010.

[6] I. Basu, K.G. Pradeep, C. Mießen, L.A. Barrales-Mora, T. Al-Samman, The role of atomic scale segregation in designing highly ductile magnesium alloys, Acta Mater. 116 (2016) 77–94. https://doi.org/10.1016/j.actamat.2016.06.024.